Improved measurement of the absolute branching fraction of inclusive semileptonic Λ_c^+ decay

M. Ablikim,[1] M. N. Achasov,[11,b] P. Adlarson,[70] M. Albrecht,[4] R. Aliberti,[31] A. Amoroso,[69a,69c] M. R. An,[35] Q. An,[66,53] X. H. Bai,[61] Y. Bai,[52] O. Bakina,[32] R. Baldini Ferroli,[26a] I. Balossino,[27a] Y. Ban,[42,g] V. Batozskaya,[1,40] D. Becker,[31] K. Begzsuren,[29] N. Berger,[31] M. Bertani,[26a] D. Bettoni,[27a] F. Bianchi,[69a,69c] J. Bloms,[63] A. Bortone,[69a,69c] I. Boyko,[32] R. A. Briere,[5] A. Brueggemann,[63] H. Cai,[71] X. Cai,[1,53] A. Calcaterra,[26a] G. F. Cao,[1,58] N. Cao,[1,58] S. A. Cetin,[57a] J. F. Chang,[1,53] W. L. Chang,[1,58] G. Chelkov,[32,a] C. Chen,[39] Chao Chen,[50] G. Chen,[1] H. S. Chen,[1,58] M. L. Chen,[1,53] S. J. Chen,[38] S. M. Chen,[56] T. Chen,[1] X. R. Chen,[28,58] X. T. Chen,[1] Y. B. Chen,[1,53] Z. J. Chen,[23,h] W. S. Cheng,[69c] S. K. Choi,[50] X. Chu,[39] G. Cibinetto,[27a] F. Cossio,[69c] J. J. Cui,[45] H. L. Dai,[1,53] J. P. Dai,[73] A. Dbeyssi,[17] R. E. de Boer,[4] D. Dedovich,[32] Z. Y. Deng,[1] A. Denig,[31] I. Denysenko,[32] M. Destefanis,[69a,69c] F. De Mori,[69a,69c] Y. Ding,[36] J. Dong,[1,53] L. Y. Dong,[1,58] M. Y. Dong,[1,53,58] X. Dong,[71] S. X. Du,[75] P. Egorov,[32,a] Y. L. Fan,[71] J. Fang,[1,53] S. S. Fang,[1,58] W. X. Fang,[1] Y. Fang,[1] R. Farinelli,[27a] L. Fava,[69b,69c] F. Feldbauer,[4] G. Felici,[26a] C. Q. Feng,[66,53] J. H. Feng,[54] K. Fischer,[64] M. Fritsch,[4] C. Fritzsch,[63] C. D. Fu,[1] H. Gao,[58] Y. N. Gao,[42,g] Yang Gao,[66,53] S. Garbolino,[69c] I. Garzia,[27a,27b] P. T. Ge,[71] Z. W. Ge,[38] C. Geng,[54] E. M. Gersabeck,[62] A. Gilman,[64] K. Goetzen,[12] L. Gong,[36] W. X. Gong,[1,53] W. Gradl,[31] M. Greco,[69a,69c] L. M. Gu,[38] M. H. Gu,[1,53] Y. T. Gu,[14] C. Y. Guan,[1,58] A. Q. Guo,[28,58] L. B. Guo,[37] R. P. Guo,[44] Y. P. Guo,[10,f] A. Guskov,[32,a] T. T. Han,[45] W. Y. Han,[35] X. Q. Hao,[18] F. A. Harris,[60] K. K. He,[50] K. L. He,[1,58] F. H. Heinsius,[4] C. H. Heinz,[31] Y. K. Heng,[1,53,58] C. Herold,[55] M. Himmelreich,[31,d] G. Y. Hou,[1,58] Y. R. Hou,[58] Z. L. Hou,[1] H. M. Hu,[1,58] J. F. Hu,[51,i] T. Hu,[1,53,58] Y. Hu,[1] G. S. Huang,[66,53] K. X. Huang,[54] L. Q. Huang,[28,58] X. T. Huang,[45] Y. P. Huang,[1] Z. Huang,[42,g] T. Hussain,[68] N. Hüsken,[25,31] W. Imoehl,[25] M. Irshad,[66,53] J. Jackson,[25] S. Jaeger,[4] S. Janchiv,[29] E. Jang,[50] J. H. Jeong,[50] Q. Ji,[1] Q. P. Ji,[18] X. B. Ji,[1,58] X. L. Ji,[1,53] Y. Y. Ji,[45] Z. K. Jia,[66,53] H. B. Jiang,[45] S. S. Jiang,[35] X. S. Jiang,[1,53,58] Y. Jiang,[58] J. B. Jiao,[45] Z. Jiao,[21] S. Jin,[38] Y. Jin,[61] M. Q. Jing,[1,58] T. Johansson,[70] N. Kalantar-Nayestanaki,[59] X. S. Kang,[36] R. Kappert,[59] B. C. Ke,[75] I. K. Keshk,[4] A. Khoukaz,[63] R. Kiuchi,[1] R. Kliemt,[12] L. Koch,[33] O. B. Kolcu,[57a] B. Kopf,[4] M. Kuemmel,[4] M. Kuessner,[4] A. Kupsc,[40,70] W. Kühn,[33] J. J. Lane,[62] J. S. Lange,[33] P. Larin,[17] A. Lavania,[24] L. Lavezzi,[69a,69c] Z. H. Lei,[66,53] H. Leithoff,[31] M. Lellmann,[31] T. Lenz,[31] C. Li,[43] C. Li,[39] C. H. Li,[35] Cheng Li,[66,53] D. M. Li,[75] F. Li,[1,53] G. Li,[1] H. Li,[47] H. Li,[66,53] H. B. Li,[1,58] H. J. Li,[18] H. N. Li,[51,i] J. Q. Li,[4] J. S. Li,[54] J. W. Li,[45] Ke Li,[1] L. J. Li,[1] L. K. Li,[1] Lei Li,[76,3] M. H. Li,[39] P. R. Li,[34,j,k] S. X. Li,[10] S. Y. Li,[56] T. Li,[45] W. D. Li,[1,58] W. G. Li,[1] X. H. Li,[66,53] X. L. Li,[45] Xiaoyu Li,[1,58] Z. X. Li,[14] H. Liang,[66,53] H. Liang,[1,58] H. Liang,[30] Y. F. Liang,[49] Y. T. Liang,[28,58] G. R. Liao,[13] L. Z. Liao,[45] J. Libby,[24] A. Limphirat,[55] C. X. Lin,[54] D. X. Lin,[28,58] T. Lin,[1] B. J. Liu,[1] C. X. Liu,[1] D. Liu,[17,66] F. H. Liu,[48] Fang Liu,[1] Feng Liu,[6] G. M. Liu,[51,i] H. Liu,[34,j,k] H. B. Liu,[14] H. M. Liu,[1,58] Huanhuan Liu,[1] Huihui Liu,[19] J. B. Liu,[66,53] J. L. Liu,[67] J. Y. Liu,[1,58] K. Liu,[1] K. Y. Liu,[36] Ke Liu,[20] L. Liu,[66,53] Lu Liu,[39] M. H. Liu,[10,f] P. L. Liu,[1] Q. Liu,[58] S. B. Liu,[66,53] T. Liu,[10,f] W. K. Liu,[39] W. M. Liu,[66,53] X. Liu,[34,j,k] Y. Liu,[34,j,k] Y. B. Liu,[39] Z. A. Liu,[1,53,58] Z. Q. Liu,[45] X. C. Lou,[1,53,58] F. X. Lu,[54] H. J. Lu,[21] J. G. Lu,[1,53] X. L. Lu,[1] Y. Lu,[7] Y. P. Lu,[1,53] Z. H. Lu,[1] C. L. Luo,[37] M. X. Luo,[74] T. Luo,[10,f] X. L. Luo,[1,53] X. R. Lyu,[58] Y. F. Lyu,[39] F. C. Ma,[36] H. L. Ma,[1] L. L. Ma,[45] M. M. Ma,[1,58] Q. M. Ma,[1] R. Q. Ma,[1,58] R. T. Ma,[58] X. Y. Ma,[1,53] Y. Ma,[42,g] F. E. Maas,[17] M. Maggiora,[69a,69c] S. Maldaner,[4] S. Malde,[64] Q. A. Malik,[68] A. Mangoni,[26b] Y. J. Mao,[42,g] Z. P. Mao,[1] S. Marcello,[69a,69c] Z. X. Meng,[61] G. Mezzadri,[27a] H. Miao,[1] T. J. Min,[38] R. E. Mitchell,[25] X. H. Mo,[1,53,58] N. Yu. Muchnoi,[11,b] Y. Nefedov,[32] F. Nerling,[17,d] I. B. Nikolaev,[11,b] Z. Ning,[1,53] S. Nisar,[9,l] Y. Niu,[45] S. L. Olsen,[58] Q. Ouyang,[1,53,58] S. Pacetti,[26b,26c] X. Pan,[10,f] Y. Pan,[52] A. Pathak,[30] M. Pelizaeus,[4] H. P. Peng,[66,53] K. Peters,[12,d] J. L. Ping,[37] R. G. Ping,[1,58] S. Plura,[31] S. Pogodin,[32] V. Prasad,[66,53] F. Z. Qi,[1] H. Qi,[66,53] H. R. Qi,[56] M. Qi,[38] T. Y. Qi,[10,f] S. Qian,[1,53] W. B. Qian,[58] Z. Qian,[54] C. F. Qiao,[58] J. J. Qin,[67] L. Q. Qin,[13] X. P. Qin,[10,f] X. S. Qin,[45] Z. H. Qin,[1,53] J. F. Qiu,[1] S. Q. Qu,[39] S. Q. Qu,[56] K. H. Rashid,[68] C. F. Redmer,[31] K. J. Ren,[35] A. Rivetti,[69c] V. Rodin,[59] M. Rolo,[69c] G. Rong,[1,58] Ch. Rosner,[17] S. N. Ruan,[39] H. S. Sang,[66] A. Sarantsev,[32,c] Y. Schelhaas,[31] C. Schnier,[4] K. Schoenning,[70] M. Scodeggio,[27a,27b] K. Y. Shan,[10,f] W. Shan,[22] X. Y. Shan,[66,53] J. F. Shangguan,[50] L. G. Shao,[1,58] M. Shao,[66,53] C. P. Shen,[10,f] H. F. Shen,[1,58] X. Y. Shen,[1,58] B. A. Shi,[58] H. C. Shi,[66,53] J. Y. Shi,[1] q. q. Shi,[50] R. S. Shi,[1,58] X. Shi,[1,53] X. D. Shi,[66,53] J. J. Song,[18] W. M. Song,[30,1] Y. X. Song,[42,g] S. Sosio,[69a,69c] S. Spataro,[69a,69c] F. Stieler,[31] K. X. Su,[71] P. P. Su,[50] Y. J. Su,[58] G. X. Sun,[1] H. Sun,[58] H. K. Sun,[1] J. F. Sun,[18] L. Sun,[71] S. S. Sun,[1,58] T. Sun,[1,58] W. Y. Sun,[30] X. Sun,[23,h] Y. J. Sun,[66,53] Y. Z. Sun,[1] Z. T. Sun,[45] Y. H. Tan,[71] Y. X. Tan,[66,53] C. J. Tang,[49] G. Y. Tang,[1] J. Tang,[54] L. Y. Tao,[67] Q. T. Tao,[23,h] M. Tat,[64] J. X. Teng,[66,53] V. Thoren,[70] W. H. Tian,[47] Y. Tian,[28,58] I. Uman,[57b] B. Wang,[1] B. L. Wang,[58] C. W. Wang,[38] D. Y. Wang,[42,g] F. Wang,[67] H. J. Wang,[34,j,k] H. P. Wang,[1,58] K. Wang,[1,53] L. L. Wang,[1] M. Wang,[45] M. Z. Wang,[42,g] Meng Wang,[1,58] S. Wang,[13] S. Wang,[10,f] T. Wang,[10,f] T. J. Wang,[39] W. Wang,[54] W. H. Wang,[71] W. P. Wang,[66,53] X. Wang,[42,g] X. F. Wang,[34,j,k] X. L. Wang,[10,f] Y. Wang,[56] Y. D. Wang,[41] Y. F. Wang,[1,53,58] Y. H. Wang,[43] Y. Q. Wang,[1] Yaqian Wang,[16,1] Z. Wang,[1,53] Z. Y. Wang,[1,58] Ziyi Wang,[58] D. H. Wei,[13] F. Weidner,[63] S. P. Wen,[1] D. J. White,[62] U. Wiedner,[4] G. Wilkinson,[64] M. Wolke,[70] L. Wollenberg,[4] J. F. Wu,[1,58] L. H. Wu,[1] L. J. Wu,[1,58] X. Wu,[10,f]

X. H. Wu,[30] Y. Wu,[66] Z. Wu,[1,53] L. Xia,[66,53] T. Xiang,[42,g] D. Xiao,[34,j,k] G. Y. Xiao,[38] H. Xiao,[10,f] S. Y. Xiao,[1] Y. L. Xiao,[10,f] Z. J. Xiao,[37] C. Xie,[38] X. H. Xie,[42,g] Y. Xie,[45] Y. G. Xie,[1,53] Y. H. Xie,[6] Z. P. Xie,[66,53] T. Y. Xing,[1,58] C. F. Xu,[1] C. J. Xu,[54] G. F. Xu,[1] H. Y. Xu,[61] Q. J. Xu,[15] X. P. Xu,[50] Y. C. Xu,[58] Z. P. Xu,[38] F. Yan,[10,f] L. Yan,[10,f] W. B. Yan,[66,53] W. C. Yan,[75] H. J. Yang,[46,e] H. L. Yang,[30] H. X. Yang,[1] L. Yang,[47] S. L. Yang,[58] Tao Yang,[1] Y. F. Yang,[39] Y. X. Yang,[1,58] Yifan Yang,[1,58] M. Ye,[1,53] M. H. Ye,[8] J. H. Yin,[1] Z. Y. You,[54] B. X. Yu,[1,53,58] C. X. Yu,[39] G. Yu,[1,58] T. Yu,[67] X. D. Yu,[42,g] C. Z. Yuan,[1,58] L. Yuan,[2] S. C. Yuan,[1] X. Q. Yuan,[1] Y. Yuan,[1,58] Z. Y. Yuan,[54] C. X. Yue,[35] A. A. Zafar,[68] F. R. Zeng,[45] X. Zeng,[6] Y. Zeng,[23,h] Y. H. Zhan,[54] A. Q. Zhang,[1] B. L. Zhang,[1] B. X. Zhang,[1] D. H. Zhang,[39] G. Y. Zhang,[18] H. Zhang,[66] H. H. Zhang,[30] H. H. Zhang,[54] H. Y. Zhang,[1,53] J. L. Zhang,[72] J. Q. Zhang,[37] J. W. Zhang,[1,53,58] J. X. Zhang,[34,j,k] J. Y. Zhang,[1] J. Z. Zhang,[1,58] Jianyu Zhang,[1,58] Jiawei Zhang,[1,58] L. M. Zhang,[56] L. Q. Zhang,[54] Lei Zhang,[38] P. Zhang,[1] Q. Y. Zhang,[35,75] Shuihan Zhang,[1,58] Shulei Zhang,[23,h] X. D. Zhang,[41] X. M. Zhang,[1] X. Y. Zhang,[45] X. Y. Zhang,[50] Y. Zhang,[64] Y. T. Zhang,[75] Y. H. Zhang,[1,53] Yan Zhang,[66,53] Yao Zhang,[1] Z. H. Zhang,[1] Z. Y. Zhang,[71] Z. Y. Zhang,[39] G. Zhao,[1] J. Zhao,[35] J. Y. Zhao,[1,58] J. Z. Zhao,[1,53] Lei Zhao,[66,53] Ling Zhao,[1] M. G. Zhao,[39] Q. Zhao,[1] S. J. Zhao,[75] Y. B. Zhao,[1,53] Y. X. Zhao,[28,58] Z. G. Zhao,[66,53] A. Zhemchugov,[32,a] B. Zheng,[67] J. P. Zheng,[1,53] Y. H. Zheng,[58] B. Zhong,[37] C. Zhong,[67] X. Zhong,[54] H. Zhou,[45] L. P. Zhou,[1,58] X. Zhou,[71] X. K. Zhou,[58] X. R. Zhou,[66,53] X. Y. Zhou,[35] Y. Z. Zhou,[10,f] J. Zhu,[39] K. Zhu,[1] K. J. Zhu,[1,53,58] L. X. Zhu,[58] S. H. Zhu,[65] S. Q. Zhu,[38] T. J. Zhu,[72] W. J. Zhu,[10,f] Y. C. Zhu,[66,53] Z. A. Zhu,[1,58] B. S. Zou,[1] and J. H. Zou[1]

(BESIII Collaboration)

[1]*Institute of High Energy Physics, Beijing 100049, People's Republic of China*
[2]*Beihang University, Beijing 100191, People's Republic of China*
[3]*Beijing Institute of Petrochemical Technology, Beijing 102617, People's Republic of China*
[4]*Bochum Ruhr-University, D-44780 Bochum, Germany*
[5]*Carnegie Mellon University, Pittsburgh, Pennsylvania 15213, USA*
[6]*Central China Normal University, Wuhan 430079, People's Republic of China*
[7]*Central South University, Changsha 410083, People's Republic of China*
[8]*China Center of Advanced Science and Technology, Beijing 100190, People's Republic of China*
[9]*COMSATS University Islamabad, Lahore Campus, Defence Road, Off Raiwind Road, 54000 Lahore, Pakistan*
[10]*Fudan University, Shanghai 200433, People's Republic of China*
[11]*G.I. Budker Institute of Nuclear Physics SB RAS (BINP), Novosibirsk 630090, Russia*
[12]*GSI Helmholtzcentre for Heavy Ion Research GmbH, D-64291 Darmstadt, Germany*
[13]*Guangxi Normal University, Guilin 541004, People's Republic of China*
[14]*Guangxi University, Nanning 530004, People's Republic of China*
[15]*Hangzhou Normal University, Hangzhou 310036, People's Republic of China*
[16]*Hebei University, Baoding 071002, People's Republic of China*
[17]*Helmholtz Institute Mainz, Staudinger Weg 18, D-55099 Mainz, Germany*
[18]*Henan Normal University, Xinxiang 453007, People's Republic of China*
[19]*Henan University of Science and Technology, Luoyang 471003, People's Republic of China*
[20]*Henan University of Technology, Zhengzhou 450001, People's Republic of China*
[21]*Huangshan College, Huangshan 245000, People's Republic of China*
[22]*Hunan Normal University, Changsha 410081, People's Republic of China*
[23]*Hunan University, Changsha 410082, People's Republic of China*
[24]*Indian Institute of Technology Madras, Chennai 600036, India*
[25]*Indiana University, Bloomington, Indiana 47405, USA*
[26a]*INFN Laboratori Nazionali di Frascati, I-00044, Frascati, Italy*
[26b]*INFN Sezione di Perugia, I-06100, Perugia, Italy*
[26c]*University of Perugia, I-06100, Perugia, Italy*
[27a]*INFN Sezione di Ferrara, I-44122, Ferrara, Italy*
[27b]*University of Ferrara, I-44122, Ferrara, Italy*
[28]*Institute of Modern Physics, Lanzhou 730000, People's Republic of China*
[29]*Institute of Physics and Technology, Peace Avenue 54B, Ulaanbaatar 13330, Mongolia*
[30]*Jilin University, Changchun 130012, People's Republic of China*
[31]*Johannes Gutenberg University of Mainz, Johann-Joachim-Becher-Weg 45, D-55099 Mainz, Germany*
[32]*Joint Institute for Nuclear Research, 141980 Dubna, Moscow region, Russia*
[33]*Justus-Liebig-Universitaet Giessen, II. Physikalisches Institut, Heinrich-Buff-Ring 16, D-35392 Giessen, Germany*
[34]*Lanzhou University, Lanzhou 730000, People's Republic of China*

[35]Liaoning Normal University, Dalian 116029, People's Republic of China
[36]Liaoning University, Shenyang 110036, People's Republic of China
[37]Nanjing Normal University, Nanjing 210023, People's Republic of China
[38]Nanjing University, Nanjing 210093, People's Republic of China
[39]Nankai University, Tianjin 300071, People's Republic of China
[40]National Centre for Nuclear Research, Warsaw 02-093, Poland
[41]North China Electric Power University, Beijing 102206, People's Republic of China
[42]Peking University, Beijing 100871, People's Republic of China
[43]Qufu Normal University, Qufu 273165, People's Republic of China
[44]Shandong Normal University, Jinan 250014, People's Republic of China
[45]Shandong University, Jinan 250100, People's Republic of China
[46]Shanghai Jiao Tong University, Shanghai 200240, People's Republic of China
[47]Shanxi Normal University, Linfen 041004, People's Republic of China
[48]Shanxi University, Taiyuan 030006, People's Republic of China
[49]Sichuan University, Chengdu 610064, People's Republic of China
[50]Soochow University, Suzhou 215006, People's Republic of China
[51]South China Normal University, Guangzhou 510006, People's Republic of China
[52]Southeast University, Nanjing 211100, People's Republic of China
[53]State Key Laboratory of Particle Detection and Electronics,
Beijing 100049, Hefei 230026, People's Republic of China
[54]Sun Yat-Sen University, Guangzhou 510275, People's Republic of China
[55]Suranaree University of Technology, University Avenue 111, Nakhon Ratchasima 30000, Thailand
[56]Tsinghua University, Beijing 100084, People's Republic of China
[57a]Turkish Accelerator Center Particle Factory Group, Istinye University, 34010, Istanbul, Turkey;
[57b]Turkish Accelerator Center Particle Factory Group, Near East University,
Nicosia, North Cyprus, Mersin 10, Turkey
[58]University of Chinese Academy of Sciences, Beijing 100049, People's Republic of China
[59]University of Groningen, NL-9747 AA Groningen, The Netherlands
[60]University of Hawaii, Honolulu, Hawaii 96822, USA
[61]University of Jinan, Jinan 250022, People's Republic of China
[62]University of Manchester, Oxford Road, Manchester, M13 9PL, United Kingdom
[63]University of Muenster, Wilhelm-Klemm-Strasse 9, 48149 Muenster, Germany
[64]University of Oxford, Keble Road, Oxford OX13RH, United Kingdom
[65]University of Science and Technology Liaoning, Anshan 114051, People's Republic of China
[66]University of Science and Technology of China, Hefei 230026, People's Republic of China
[67]University of South China, Hengyang 421001, People's Republic of China
[68]University of the Punjab, Lahore 54590, Pakistan
[69a]University of Turin, I-10125, Turin, Italy
[69b]University of Eastern Piedmont, I-15121, Alessandria, Italy
[69c]INFN, I-10125, Turin, Italy
[70]Uppsala University, Box 516, SE-75120 Uppsala, Sweden
[71]Wuhan University, Wuhan 430072, People's Republic of China
[72]Xinyang Normal University, Xinyang 464000, People's Republic of China
[73]Yunnan University, Kunming 650500, People's Republic of China
[74]Zhejiang University, Hangzhou 310027, People's Republic of China
[75]Zhengzhou University, Zhengzhou 450001, People's Republic of China
[76]Renmin University of China, Beijing 100872, People's Republic of China

[a]Also at the Moscow Institute of Physics and Technology, Moscow 141700, Russia.
[b]Also at the Novosibirsk State University, Novosibirsk, 630090, Russia.
[c]Also at the NRC "Kurchatov Institute," PNPI, 188300, Gatchina, Russia.
[d]Also at Goethe University Frankfurt, 60323 Frankfurt am Main, Germany.
[e]Also at Key Laboratory for Particle Physics, Astrophysics and Cosmology, Ministry of Education; Shanghai Key Laboratory for Particle Physics and Cosmology; and Institute of Nuclear and Particle Physics, Shanghai 200240, People's Republic of China.
[f]Also at Key Laboratory of Nuclear Physics and Ion-beam Application (MOE) and Institute of Modern Physics, Fudan University, Shanghai 200443, People's Republic of China.
[g]Also at State Key Laboratory of Nuclear Physics and Technology, Peking University, Beijing 100871, People's Republic of China.
[h]Also at School of Physics and Electronics, Hunan University, Changsha 410082, China.
[i]Also at Guangdong Provincial Key Laboratory of Nuclear Science, Institute of Quantum Matter, South China Normal University, Guangzhou 510006, China.
[j]Also at Frontiers Science Center for Rare Isotopes, Lanzhou University, Lanzhou 730000, People's Republic of China.

(Received 7 December 2022; accepted 27 February 2023; published 17 March 2023)

Using 4.5 fb^{-1} of e^+e^- annihilation data samples collected at center-of-mass energies ranging from 4.600 to 4.698 GeV with the BESIII detector at the BEPCII collider, we measured the absolute branching fraction for the inclusive semileptonic decay $\Lambda_c^+ \to Xe^+\nu_e$, where X refers to any possible particle system. The branching fraction of the decay is determined to be $\mathcal{B}(\Lambda_c^+ \to Xe^+\nu_e) = (4.06 \pm 0.10_{\rm stat} \pm 0.09_{\rm syst})\%$. Our result improves the precision of previous measurements of $\mathcal{B}(\Lambda_c^+ \to Xe^+\nu_e)$ by more than threefold. Using the known Λ_c^+ lifetime and the charge-averaged semileptonic decay width of nonstrange charmed mesons, we measure the ratio of inclusive semileptonic decay widths $\Gamma(\Lambda_c^+ \to Xe^+\nu_e)/\bar{\Gamma}(D \to Xe^+\nu_e) = 1.28 \pm 0.05$, where statistical and systematic uncertainties are combined.

DOI: 10.1103/PhysRevD.107.052005

I. INTRODUCTION

The lowest-lying charmed baryon Λ_c^+ was discovered more than 40 years ago [1,2], but about 30% of Λ_c^+ decays are still unmeasured [3]. In recent years, great experimental progress has been made in the study of Λ_c^+ semileptonic (SL) decays [4,5]. For example, the BESIII experiment obtained a precise absolute branching fraction (BF) for the dominant semileptonic mode, $\mathcal{B}(\Lambda_c^+ \to \Lambda e^+\nu_e) = (3.56 \pm 0.11_{\rm stat} \pm 0.07_{\rm syst})\%$, and also measured the differential decay rate and form factors in this decay for the first time [6]. The $\Lambda_c^+ \to pK^-e^+\nu_e$ decay is now also observed with a significance of 8.2σ with a measured BF $\mathcal{B}(\Lambda_c^+ \to pK^-e^+\nu_e) = (0.82 \pm 0.15_{\rm stat} \pm 0.06_{\rm syst}) \times 10^{-3}$ [7]. Evidence of the $\Lambda^*(1520)$ is seen in the pK^- mass spectrum with a significance of 3.3σ [7]. In addition, the BF for the inclusive SL Λ_c^+ decay is measured to be $\mathcal{B}(\Lambda_c^+ \to Xe^+\nu_e) = (3.95 \pm 0.34_{\rm stat} \pm 0.09_{\rm syst})\%$ [8]. However, in comparison to the experimental studies of SL decays in D mesons, measurements of the SL decays in Λ_c^+ are still very limited [3].

Improved precision on $\mathcal{B}(\Lambda_c^+ \to Xe^+\nu_e)$ is desirable. First, a comparison of $\mathcal{B}(\Lambda_c^+ \to Xe^+\nu_e)$ with $\mathcal{B}(\Lambda_c^+ \to \Lambda e^+\nu_e)$ and $\mathcal{B}(\Lambda_c^+ \to pK^-e^+\nu_e)$ indicates that some new Λ_c^+ SL decays may exist beyond the known $\Lambda_c^+ \to \Lambda\ell^+\nu_\ell$ and $\Lambda_c^+ \to pK^-\ell^+\nu_\ell$ ($\ell = e,\ \mu$). Second, combining this branching fraction with the known lifetime of the Λ_c^+ baryon determines the SL decay width $\Gamma(\Lambda_c^+ \to Xe^+\nu_e)$. Comparing with the charge-averaged nonstrange D SL decay width $\bar{\Gamma}(D \to Xe^+\nu_e)$, one finds the ratio $\Gamma(\Lambda_c^+ \to Xe^+\nu_e)/\bar{\Gamma}(D \to Xe^+\nu_e) = 1.26 \pm 0.12$ [8], about a 10% uncertainty. Improving the precision on $\Gamma(\Lambda_c^+ \to Xe^+\nu_e)/\bar{\Gamma}(D \to Xe^+\nu_e)$ is helpful for testing current theoretical predictions [9–11].

This article presents an improved BF measurement of the Λ_c^+ inclusive SL decay. Our measurement is performed by using data sets collected with the BESIII detector at center-of-mass energies $\sqrt{s} = 4.600$, 4.612, 4.628, 4.640, 4.661, 4.682 and 4.698 GeV. The total integrated luminosity for these data samples is 4.5 fb^{-1} [12,13]. These are the largest data samples collected near the $\Lambda_c^+\bar{\Lambda}_c^-$ production threshold. Throughout this paper, charge-conjugate modes are implied unless explicitly noted.

II. BESIII DETECTOR AND MONTE CARLO SIMULATION

The BESIII detector [14] records symmetric e^+e^- collisions provided by the BEPCII storage ring in the center-of-mass energy range from 2.00 to 4.95 GeV, with a peak luminosity of 1×10^{33} cm^{-2} s^{-1} achieved at $\sqrt{s} = 3.77$ GeV. The BESIII spectrometer is a cylindrical detector with a solid-angle coverage of 93% of 4π. The detector consists of a helium-gas-based main drift chamber (MDC), a plastic scintillator time-of-flight (TOF) system, a CsI(Tl) electromagnetic calorimeter (EMC), a superconducting solenoid providing a 1.0 T magnetic field and a muon counter [15]. The charged-particle momentum resolution is 0.5% at a transverse momentum of 1 GeV/c, and the specific energy loss (dE/dx) resolution is 6% for the electrons from Bhabha scattering. The photon energy resolution in the EMC is 2.5% in the barrel and 5.0% in the end caps at energies of 1 GeV. The time resolution of the TOF barrel part is 68 ps, while that of the end-cap part is 110 ps. The end-cap TOF system was upgraded in 2015 with multigap resistive plate chamber technology, providing a time resolution of 60 ps [16]. About 11% of the data set was obtained before the TOF upgrade. More details about the design and performance of the detector were given in Ref. [14].

A GEANT4-based [17] Monte Carlo (MC) simulation toolkit, which includes the geometric description of the

[k]Also at Lanzhou Center for Theoretical Physics, Lanzhou University, Lanzhou 730000, People's Republic of China.
[l]Also at the Department of Mathematical Sciences, IBA, Karachi, Pakistan.

detector and the detector response, is used to determine signal detection efficiency and to estimate potential backgrounds. In the simulation, the effects of beam-energy spread and initial-state radiation [18] are incorporated using KKMC [19], and final-state radiation from charged final-state particles is incorporated using PHOTOS [20]. An inclusive MC sample consisting of $\Lambda_c^+\bar{\Lambda}_c^-$, $D_{(s)}^{(*)}\bar{D}_{(s)}^{(*)}$ pairs, radiative return to charmonium(-like) ψ states at lower masses and continuum processes of $q\bar{q}$ ($q = u,\ d,\ s$), along with Bhabha scattering, $\mu^+\mu^-$, $\tau^+\tau^-$ and $\gamma\gamma$ events are generated. All particle decays are modeled with EvtGen [21] using BFs either taken from the Particle Data Group [3], when available, or otherwise estimated with LUNDCHARM [22,23].

III. ANALYSIS

The first procedure of this analysis is to reconstruct "single-tag" (ST) events with a fully reconstructed $\bar{\Lambda}_c^-$ candidate. The $\bar{\Lambda}_c^-$ hadronic decay tag modes used in this analysis are $\bar{\Lambda}_c^- \to \bar{p}K_S^0$, $\bar{p}K^+\pi^-$, $\bar{p}K_S^0\pi^0$, $\bar{p}K^+\pi^-\pi^0$, $\bar{p}K_S^0\pi^+\pi^-$, $\bar{\Lambda}\pi^-$, $\bar{\Lambda}\pi^-\pi^0$, $\bar{\Lambda}\pi^-\pi^+\pi^-$, $\bar{\Sigma}^0\pi^-$, $\bar{\Sigma}^-\pi^0$, $\bar{\Sigma}^-\pi^+\pi^-$ and $\bar{\Sigma}^0\pi^-\pi^0$, where the intermediate particles K_S^0, $\bar{\Lambda}$, $\bar{\Sigma}^0$, $\bar{\Sigma}^-$ and π^0 are reconstructed via $K_S^0 \to \pi^+\pi^-$, $\bar{\Lambda} \to \bar{p}\pi^+$, $\bar{\Sigma}^0 \to \gamma\bar{\Lambda}$ with $\bar{\Lambda} \to \bar{p}\pi^+$, $\bar{\Sigma}^- \to \bar{p}\pi^0$ and $\pi^0 \to \gamma\gamma$, respectively. Starting with this ST sample, we identify the inclusive SL decay $\Lambda_c^+ \to Xe^+\nu_e$ candidates; selected events are referred to as the double-tag (DT) sample [24].

A. Single-tag selection

Charged tracks are required to satisfy $|\cos\theta| < 0.93$, where θ is the polar angle with respect to the z axis, which is the symmetry axis of the MDC. Their distances of the closest approach to the interaction point (IP) are required to be less than 10 cm along z axis and less than 1 cm in the transverse plane. For charged tracks originating from K_S^0, $\bar{\Lambda}$ and $\bar{\Sigma}^-$, there is no transverse requirement and a relaxed requirement of 20 cm matching along the z axis is employed. The information from the dE/dx in MDC and the flight time in the TOF are used to obtain particle identification (PID) probabilities for the pion ($\mathcal{L}_\pi$) and kaon ($\mathcal{L}_K$) hypotheses. The pion and kaon candidates are selected using $\mathcal{L}_\pi > \mathcal{L}_K$ and $\mathcal{L}_K > \mathcal{L}_\pi$, respectively. To identify protons, the information from the dE/dx, TOF, and EMC are combined to calculate the PID probability $\mathcal{L}'$. Charged tracks satisfying $\mathcal{L}'_p > \mathcal{L}'_\pi$ and $\mathcal{L}'_p > \mathcal{L}'_K$ are identified as proton candidates.

Photon candidates are identified using showers in the EMC. The deposited energy of each shower must be more than 25 MeV in the barrel region ($|\cos\theta| \le 0.80$) and more than 50 MeV in the end-cap region ($0.86 \le |\cos\theta| \le 0.92$). To exclude showers that originate from charged tracks, the angle subtended by the EMC shower and the position of the closest charged track at the EMC must be greater than 10 degrees as measured from the IP. To suppress electronic noise and showers unrelated to the event, the difference between the EMC time and the event start time is required to be within [0, 700] ns. To reconstruct π^0 candidates, the invariant mass of the accepted photon pair is required to be within $(0.110, 0.155)$ GeV/c^2. A kinematic fit is performed to constrain the $\gamma\gamma$ invariant mass to the known π^0 mass [3], and the χ^2 of the kinematic fit is required to be less than 20. The fitted momenta of the π^0 are used in the further analysis.

The K_S^0 meson is reconstructed from two oppositely charged tracks with invariant mass within $(0.485, 0.510)$ GeV/c^2. The two charged tracks are constrained to originate from a common vertex and their decay length relative to the IP is required to be larger than zero. The invariant masses $M(\bar{p}\pi^+)$, $M(\gamma\bar{\Lambda})$ and $M(\bar{p}\pi^0)$ are required to be within (1.110,1.121), (1.179, 1.205) and $(1.171, 1.204)$ GeV/c^2 to reconstruct candidates for $\bar{\Lambda}$, $\bar{\Sigma}^0$ and $\bar{\Sigma}^-$, respectively. For the ST mode $\bar{p}\pi^+\pi^-$, the backgrounds from Cabibbo-favored components of $\bar{\Lambda}\pi^-$ and $\bar{p}K_S^0$ are removed by rejecting any event with $M_{\bar{p}\pi^+} \in (1.105, 1.125)$ GeV/c^2 and $M_{\pi^+\pi^-} \in (0.475, 0.520)$ GeV/c^2.

The ST $\bar{\Lambda}_c^-$ signals are identified using the beam constrained mass:

$$M_{\rm BC} = \sqrt{(\sqrt{s}/2)^2 - |\vec{p}_{\bar{\Lambda}_c^-}|^2},$$

where $\vec{p}_{\bar{\Lambda}_c^-}$ is the measured momentum of the ST $\bar{\Lambda}_c^-$. The energy difference $\Delta E = \sqrt{s}/2 - E_{\bar{\Lambda}_c^-}$ is determined for ST $\bar{\Lambda}_c^-$ baryons, where $E_{\bar{\Lambda}_c^-}$ is the measured energy of the ST $\bar{\Lambda}_c^-$. If an event satisfies more than one $\bar{\Lambda}_c^-$ tag, only the tag with the minimum $|\Delta E|$ is kept to avoid double counting among STs (but a second tag with opposite charm is allowed). The $M_{\rm BC}$ distributions at $\sqrt{s} = 4.682$ GeV for 12 ST modes are shown in Fig. 1. Unbinned maximum likelihood fits are performed to the spectra using the MC-simulated signal shape convolved with a Gaussian function accounting for differences of resolutions between data and MC simulation to describe the signal, and an ARGUS function [25] with end point fixed at $\sqrt{s}/2$ to describe the background. The ΔE requirements, $M_{\rm BC}$ distributions for other data sets and their ST yields were documented in Refs. [6,7]. The total ST yield reconstructed in all data samples is $N_{\rm ST} = 115437 \pm 446$, where the uncertainty is statistical only.

B. Double-tag selection

In the selected ST sample of $\bar{\Lambda}_c^-$ candidates, we search for a charged track identified as a positron in the recoiling system of ST $\bar{\Lambda}_c^-$ baryons. The charged track is required to have $|\cos\theta| < 0.80$ to ensure that the track lies within the barrel of the EMC, which has better energy resolution than the EMC end caps. The distance of the closest approach to the IP is required to be less than 10 cm along the z axis and

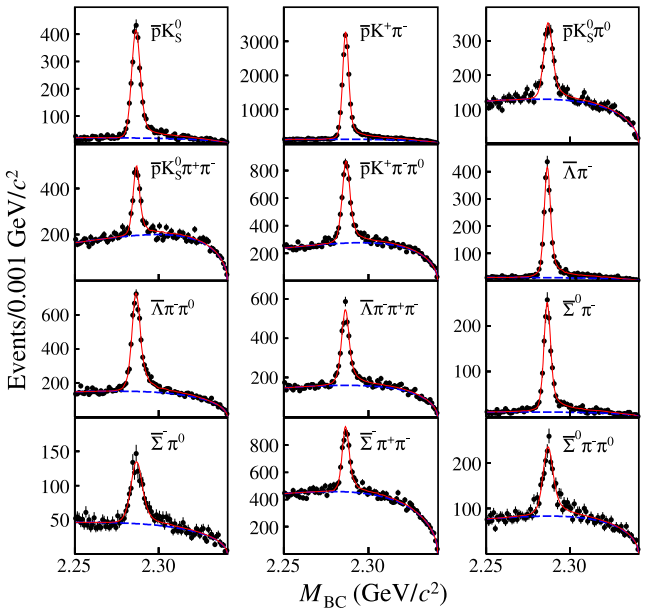

FIG. 1. Fits to the $M_{\rm BC}$ distributions for different ST modes at $\sqrt{s} = 4.682$ GeV. The points with error bars are data, the (red) solid curves show the total fits and the (blue) dashed curves are the fitted backgrounds.

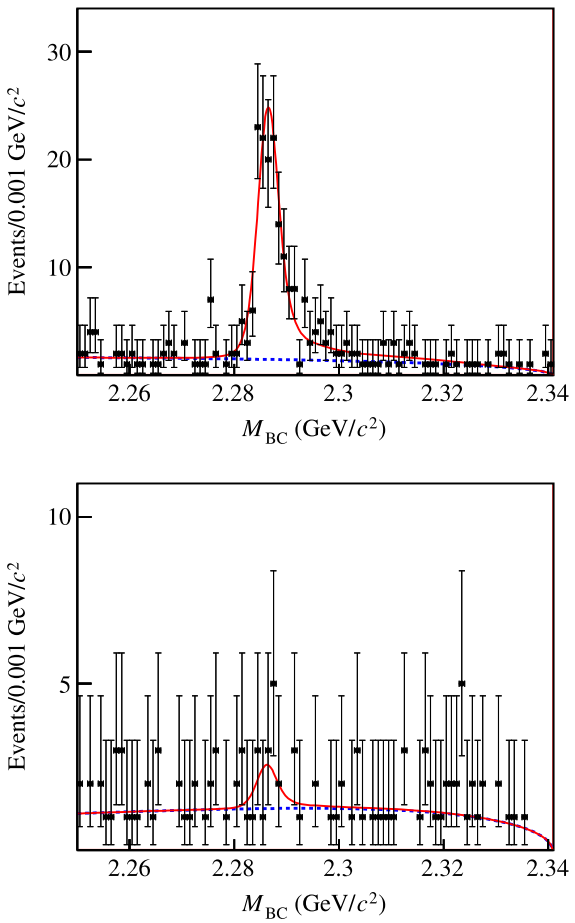

FIG. 2. Example $M_{\rm BC}$ fits for double-tag RS (upper) and WS (lower) positron candidates with momentum in the range 500–550 MeV/c for data collected at $\sqrt{s} = 4.682$ GeV. The points with error bars are data, the (red) solid curves show the total fits and the (blue) dashed curves are the fitted backgrounds.

less than 1 cm in the transverse plane. The track is required to have momentum above 200 MeV/c since PID is difficult at low momenta.

We sort the selected recoil-side positron candidates into 16 50 MeV/c momentum bins between 200 MeV/c and 1000 MeV/c. For a given momentum bin, the selected charged tracks are divided into two charge categories: the right-sign (RS) and wrong-sign (WS) samples, where the charge of the RS (WS) track is required to be opposite (equal) to that of the ST $\bar{\Lambda}_c^-$ candidate. Here, the WS samples are used to determine the charge-symmetric backgrounds in the RS samples. For both charge categories in each of the momentum bins, the charged tracks are then sorted into four mutually exclusive PID hypotheses: positron, pion, kaon and proton. The PID of each selected charged track is implemented with the information measured from the dE/dx, TOF and EMC, and the combined likelihoods for positron, pion, kaon and proton hypotheses ($\mathcal{L}'_e$, $\mathcal{L}'_\pi$, $\mathcal{L}'_K$ and $\mathcal{L}'_p$) are calculated. The positron candidate must satisfy $\mathcal{L}'_e > 0.001$ and $\mathcal{L}'_e/(\mathcal{L}'_e + \mathcal{L}'_\pi + \mathcal{L}'_K) > 0.8$. To further suppress the background from charged hadrons, the $E_e/p_e > 0.8$ is required [8,26], where E_e and p_e are the deposited energy in the EMC and momentum value measured by the MDC, respectively. The remaining selected charged tracks are assigned to different hadron types according to the highest likelihood value that is also greater than 0.001.

For both RS and WS in a given momentum bin, we determine the number of the charged tracks originating from a Λ_c^+ by performing the unbinned fit to the $M_{\rm BC}$ distribution of the ST $\bar{\Lambda}_c^-$ candidate. Figure 2 shows two examples of the fits, where the $M_{\rm BC}$ distributions obtained from all 12 $\bar{\Lambda}_c^-$ ST hadronic decays are combined together. The reason for combining all ST modes together is that the yields of the RS and WS positrons from each of the ST modes are very limited in each of the momentum bins. From separate fits to $M_{\rm BC}$ distributions in each data set, the yields of the total RS and WS positron yields are determined to be 3706 ± 71 and 394 ± 31, respectively, where the uncertainties are statistical only. The measured yields as a function of momentum bin for each particle category are shown in Fig. 3.

C. PID unfolding

The measured positron yields in each momentum bin contain sizable backgrounds from misidentified hadrons. To evaluate these backgrounds, knowledge of their yields and corresponding identification and misidentification probabilities is required. We relate the true number of

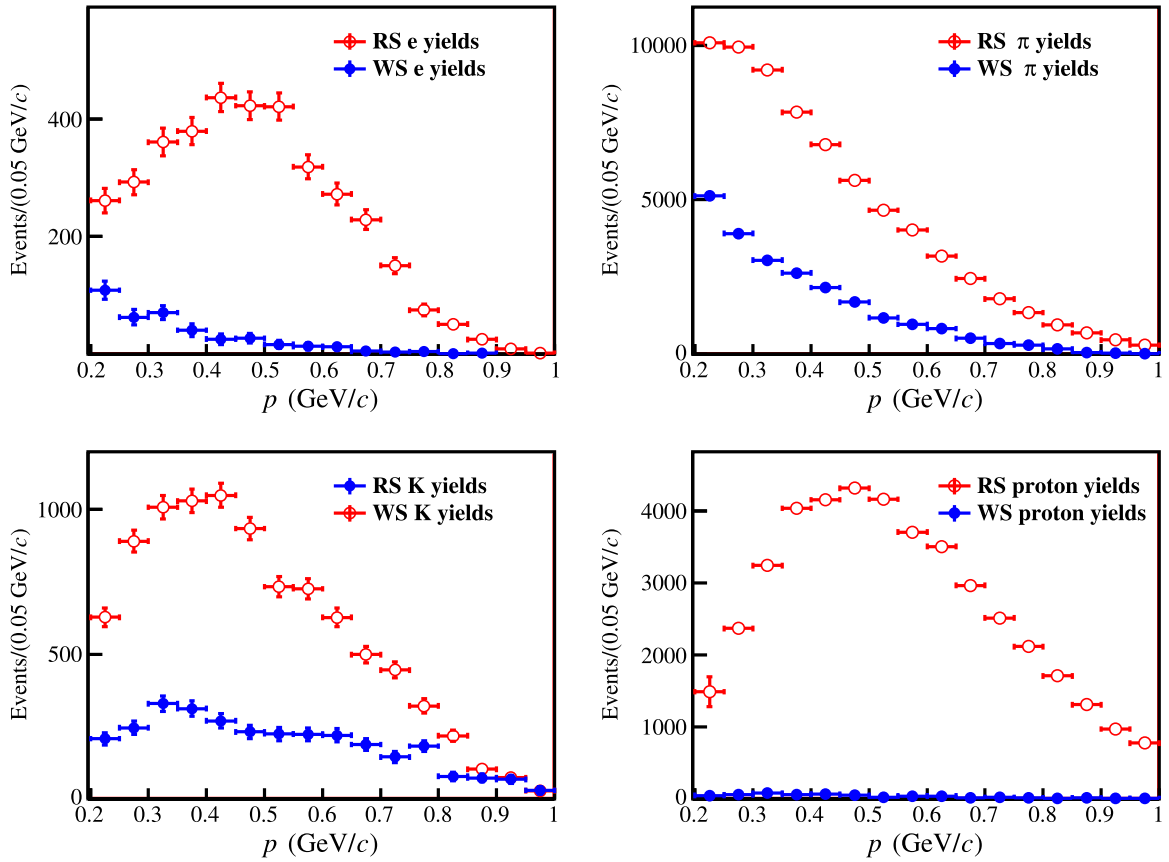

FIG. 3. Measured RS (blue) and WS (red) yields for each particle category as a function of momentum.

positrons and the observed number of positrons in DT events with a PID migration matrix ($A_{\rm PID}$):

$$\begin{bmatrix} N_e^{\rm obs} \\ N_\pi^{\rm obs} \\ N_K^{\rm obs} \\ N_p^{\rm obs} \end{bmatrix} = \begin{bmatrix} P_{e\to e} & P_{\pi\to e} & P_{K\to e} & P_{p\to e} \\ P_{e\to\pi} & P_{\pi\to\pi} & P_{K\to\pi} & P_{p\to\pi} \\ P_{e\to K} & P_{\pi\to K} & P_{K\to K} & P_{p\to K} \\ P_{e\to p} & P_{\pi\to p} & P_{K\to p} & P_{p\to p} \end{bmatrix} \begin{bmatrix} N_e^{\rm true} \\ N_\pi^{\rm true} \\ N_K^{\rm true} \\ N_p^{\rm true} \end{bmatrix}, \quad (1)$$

where $N_a^{\rm obs}$ is the observed yield of particle species a (where a denotes e, π, K or p), $P_{a\to b}$ is the efficiency of identifying particle a as particle b, and $N_a^{\rm true}$ is true yield of particle a in the studied sample. We do not attempt to separate muons; most muons will be identified as pions by our classification scheme. To obtain the elements in the PID efficiency matrix ($A_{\rm PID}$), the control samples for positrons, charged pions, kaons and protons are studied. These control samples are selected from the Λ_c^+ inclusive MC sample, by comparing the opening angle ($\Delta_{\rm angle} < 5°$) between the reconstructed charged tracks and the produced charged particles. Based on these selected control samples of positrons, pions, kaons and protons, the elements of $A_{\rm PID}$, $P_{a\to b}$, as a function of momentum are obtained. To account for the possible differences in the migration probabilities $P_{a\to b}$ between data and MC sample, corrections to $P_{a\to b}$ are applied in each momentum bin. For positrons, the difference in PID efficiency between data and MC sample is studied using the radiative Bhabha scattering process. For kaons and pions, the differences in PID efficiencies between data and MC sample are studied using the decays $J/\psi \to K^+K^-\pi^+\pi^-(\pi^0)$ and $J/\psi \to K^+K^-K^+K^-(\pi^0)$. For protons, the decay $J/\psi \to p\bar{p}\pi^+\pi^-(\pi^0)$ is analyzed. The averaged relative differences (uncertainties) are evaluated to be $-0.5(0.4)\%$, $-2.2(0.3)\%$, $-1.0(0.2)\%$ and $-2.3(0.3)\%$ for $P_{e\to e}$, $P_{\pi\to\pi}$, $P_{K\to K}$ and $P_{p\to p}$, respectively. After these corrections, the PID efficiencies for each of the charged particles as a function of momentum are shown in Fig. 4. An example of the $A_{\rm PID}$ for $0.50 < p < 0.55\,{\rm GeV}/c$ is shown in the Appendix.

We unfold PID migration effects by applying the inverse of the migration matrix to the observed RS and WS yields in each momentum bin. We obtain the true yield of RS positron tracks from Λ_c^+ decays and the true WS backgrounds, as shown in Fig. 5. We randomly Gaussian smear each observed yield with its uncertainty and repeat the unfolding procedure many times. The rms of each resulting unfolded yield is assigned as its statistical uncertainty. We then take the difference of the number of the RS positrons and WS electrons to subtract the contributions of positrons

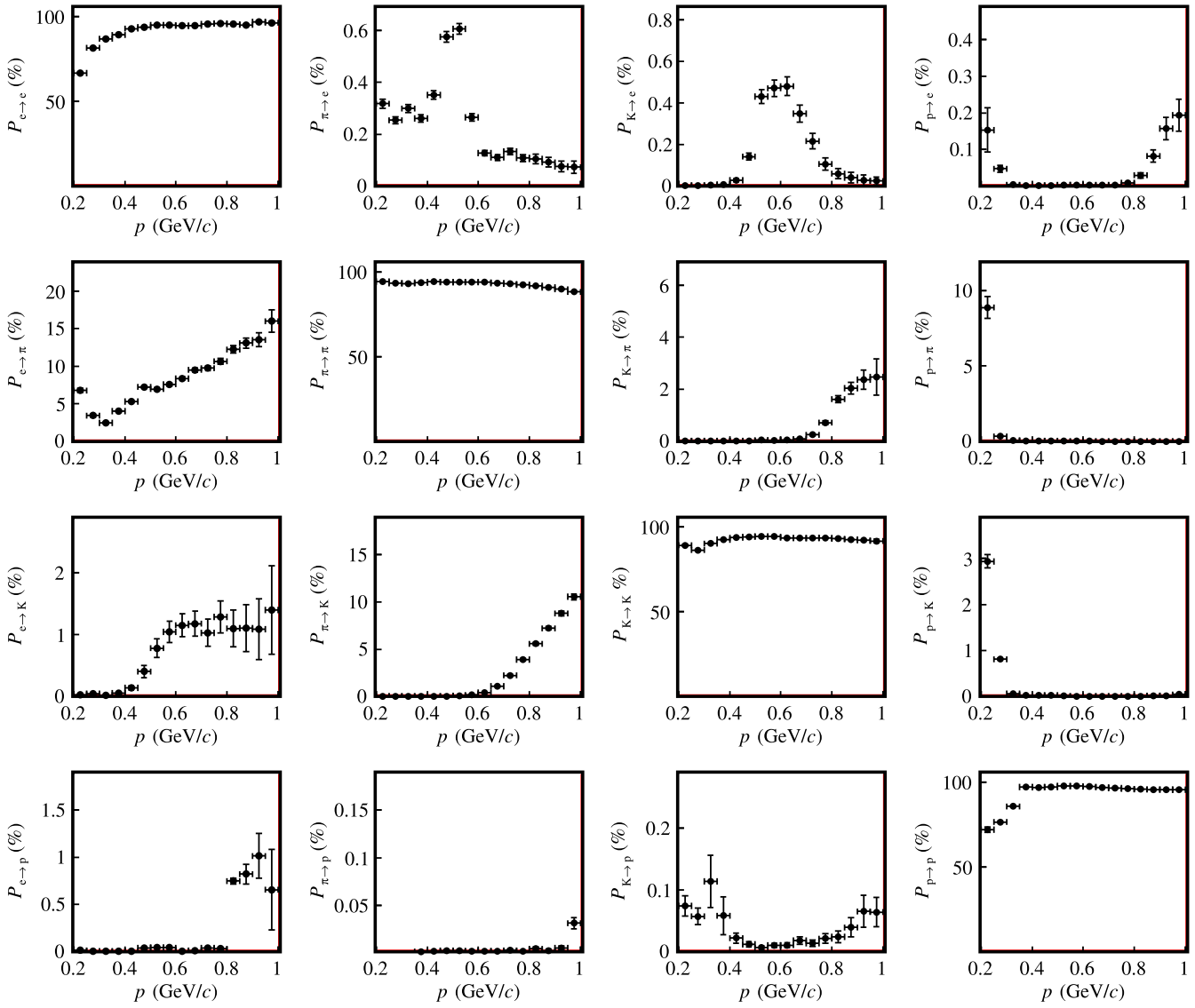

FIG. 4. PID efficiencies as a function of momentum used to populate the A_{PID} matrices.

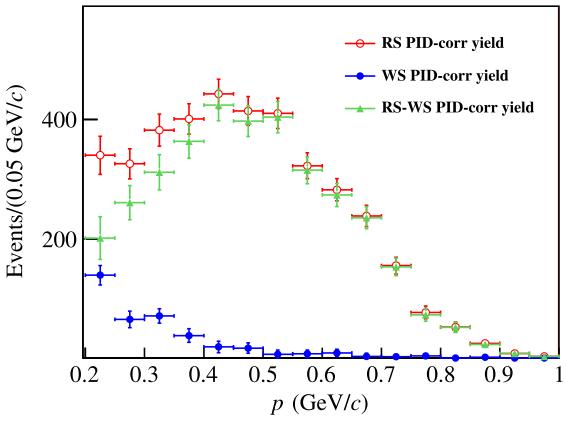

FIG. 5. PID unfolding results of positrons from $\Lambda_c^+ \to Xe^+\nu_e$ events for data sets collected between $\sqrt{s} = 4.600$ and 4.698 GeV. The RS PID-corrected yields are shown in red circles, while the WS PID-corrected yields are shown in blue dots. Their differences are shown as green triangles.

from Dalitz decays of light mesons in the final state of Λ_c^+ decay, such as $\pi^0 \to \gamma e^+ e^-$, and any other charge-symmetric backgrounds.

D. Tracking efficiency and momentum migration

To account for tracking efficiency and momentum bin migration, a second unfolding is performed using

$$N_{\mathrm{e}}^{\mathrm{true}}(i) = \sum_j A_{\mathrm{TRK}}(e|i,j) N_{\mathrm{e}}^{\mathrm{prod}}(j), \tag{2}$$

where the tracking efficiency matrix A_{TRK} describes the efficiency that positrons produced in the jth momentum bin are reconstructed in the ith momentum bin, $N_{\mathrm{e}}^{\mathrm{prod}}(j)$ is the number of primary positrons produced in the jth momentum bin, and $N_{\mathrm{e}}^{\mathrm{true}}(i)$ is the true yield of positron reconstructed in the ith momentum bin.

TABLE I. Positron yield in data after each procedure. The listed uncertainties are statistical.

Correction (see text)	RS yields	WS yields
Observed yields	3706 ± 71	394 ± 31
PID unfolding yields	3865 ± 80	376 ± 33
WS subtraction	3489 ± 87	
Tracking unfolding yields	4333 ± 107	
Extrapolation	4692 ± 117	

To determine the tracking efficiency matrix $A_{\rm TRK}$, the MC samples of one Λ_c^+ baryon decaying to $Xe^+\nu_e$ together with a $\bar{\Lambda}_c$ decaying to each ST mode are generated at each of the center-of-mass energies. The tracking efficiency of $\Lambda_c^+ \to Xe^+\nu_e$ for each ST mode is determined first and then weighted according to their ST yields. The tracking efficiency matrix $A_{\rm TRK}$ is shown in the Appendix, including the effects of geometrical acceptance ($|\cos\theta| < 0.80$), track reconstruction efficiency, and resolution smearing. Unfolding with the matrix inverse, we obtain the efficiency-corrected positron momentum spectrum above 200 MeV/c in the laboratory system. The corrected positron yield is determined to be 4333 ± 107, where the uncertainty is statistical only. The efficiency-corrected positron yields in each of the momentum bins as well as their correlation coefficients are shown in the Appendix. Table I summarizes the positron yields obtained after each correction step.

E. Branching fraction

The yield of positrons with $p_e \leq 200$ MeV/c is obtained by fitting the efficiency-corrected positron momentum spectrum with the sum of the spectra of the exclusive decay channels, as shown in Fig. 6. In the fit, the BF of each component is fixed to its central value. The details of the incorporated exclusive channels are shown in Table II. Combining with the measured yields with $p_e > 200$ MeV/c, we obtain the total efficiency-corrected yield of $\Lambda_c^+ \to Xe^+\nu_e$, $N_{\rm prod} = 4692 \pm 117$, where the uncertainty is statistical only. This allows us to calculate the BF of $\Lambda_c^+ \to Xe^+\nu_e$ by

$$\mathcal{B}(\Lambda_c^+ \to Xe^+\nu_e) = \frac{N_{\rm prod}}{N_{\rm ST}}. \quad (3)$$

Inserting $N_{\rm ST} = 115437 \pm 446$ into Eq. (3), we measure

$$\mathcal{B}(\Lambda_c^+ \to Xe^+\nu_e) = (4.06 \pm 0.10_{\rm stat} \pm 0.09_{\rm syst})\%.$$

The measured $\mathcal{B}(\Lambda_c^+ \to Xe^+\nu_e)$ is consistent with the previous result $\mathcal{B}(\Lambda_c^+ \to Xe^+\nu_e) = (3.95 \pm 0.34_{\rm stat} \pm 0.09_{\rm syst})\%$ [8], but with greatly improved precision.

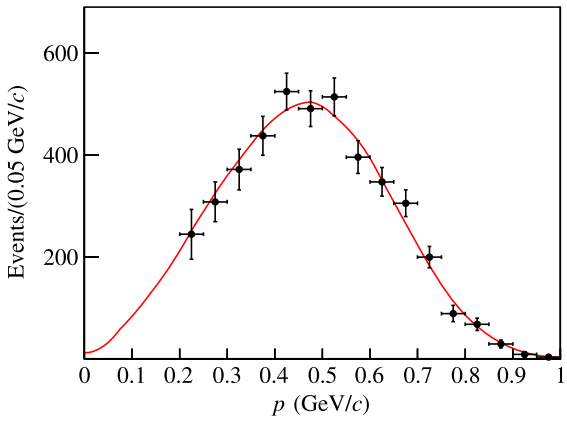

FIG. 6. Extrapolation of the positron momentum spectrum obtained from the data. The black points show data, while the red curve shows the extrapolated momentum spectrum.

TABLE II. Exclusive Λ_c^+ SL decays used to extrapolate the positron momentum spectrum. The BFs of $\Lambda_c^+ \to \Lambda e^+\nu_e$ and $\Lambda_c^+ \to pK^-e^+\nu_e$ are measured by the BESIII experiment [6,7]. The BF of $\Lambda_c^+ \to n\bar{K}^0e^+\nu_e$ is taken as the BF of $\Lambda_c^+ \to pK^-e^+\nu_e$ according to the isospin symmetry of the $N\bar{K}$ system. The form factor of the $\Lambda_c^+ \to \Lambda e^+\nu_e$ is taken from BESIII measurements [6]. The model for $\Lambda_c^+ \to pK^-(n\bar{K}^0)e^+\nu_e$ is taken as the phase space (PHSP). The BFs and models of $\Lambda_c^+ \to \Lambda(1405)e^+\nu_e$ and $\Lambda_c^+ \to \Lambda(1520)e^+\nu_e$ are taken from the predictions in Refs. [27,28], while the BF and model of $\Lambda_c^+ \to ne^+\nu_e$ are taken from Ref. [29].

Decay	$\mathcal{B}$ [%]	Model
$\Lambda_c^+ \to \Lambda e^+\nu_e$	$3.56 \pm 0.11 \pm 0.07$	References [6]
$\Lambda_c^+ \to pK^-(n\bar{K}^0)e^+\nu_e$	$0.088 \pm 0.017 \pm 0.007$	PHSP [7]
$\Lambda_c^+ \to \Lambda(1405)e^+\nu_e$	0.24	HQET [27,28]
$\Lambda_c^+ \to \Lambda(1520)e^+\nu_e$	0.06	HQET [27,28]
$\Lambda_c^+ \to ne^+\nu_e$	0.20	Quark model [29]

F. Systematic uncertainty

The systematic uncertainties in measuring $\mathcal{B}(\Lambda_c^+ \to Xe^+\nu_e)$ are listed in Table III. The uncertainty in the tracking efficiency of positrons is evaluated at 0.4% from studies of $e^+e^- \to (\gamma)e^+e^-$ events. The systematic uncertainty in the ST yields is estimated to be 1.0% studied using alternative signal and background shapes [6]. The systematic uncertainty due to the $A_{\rm PID}$ and $A_{\rm TRK}$ matrices is estimated by randomly Gaussian smearing all elements of these matrices 300 times, based on their errors, and

TABLE III. Sources of the systematic uncertainties in measuring $\mathcal{B}(\Lambda_c^+ \to Xe^+\nu_e)$.

Source	Value (%)
Tracking efficiency for positron	0.4
ST signal shape	1.0
$A_{\rm PID}$ and $A_{\rm TRK}$ matrices	0.9
Momentum extrapolation	1.6
ST Yields method for RS and WS positrons	0.6
Muon contamination treatment	0.2
Total	2.2

redetermining the BF. The 0.9% width of the resulting distribution of these BF results is taken as the systematic uncertainty. The systematic uncertainty in the extrapolation of the positron momentum spectrum is estimated by varying the BFs of $\Lambda_c^+ \to \Lambda e^+\nu_e$, $\Lambda_c^+ \to pK^-e^+\nu_e$, $\Lambda_c^+ \to n\bar{K}^0e^+\nu_e$, $\Lambda_c^+ \to \Lambda(1405)e^+\nu_e$, $\Lambda_c^+ \to \Lambda(1520)e^+\nu_e$ and $\Lambda_c^+ \to ne^+\nu_e$. The BFs of $\Lambda_c^+ \to \Lambda e^+\nu_e$ and $\Lambda_c^+ \to pK^-(n\bar{K}^0)e^+\nu_e$ are varied by one standard deviation according to measurements [6,7]. The BFs for $\Lambda_c^+ \to \Lambda(1405)e^+\nu_e$ and $\Lambda_c^+ \to \Lambda(1520)e^+\nu_e$ are varied from 0.24% to 0.38%, and from 0.06% to 0.08% according to predictions in Refs. [27,28]. The BF for $\Lambda_c^+ \to ne^+\nu_e$ is varied from 0.2% to 0.4% according to predictions in Refs. [28–34]. In addition, there may be multibody decays like $\Lambda_c^+ \to \Lambda\pi^0e^+\nu_e$, $\Lambda_c^+ \to \Lambda\pi^+\pi^-e^+\nu_e$, etc. In the absence of data or predictions, the BFs of these decays are both taken as the conservatively large value 0.2%. With these exclusive BFs varied one by one in alternative fits, the signal shape is reformed and the $\mathcal{B}(\Lambda_c^+ \to Xe^+\nu_e)$ is obtained. The largest relative difference, 1.6%, between the new measured BF and the nominal one is taken as the systematic uncertainty due to momentum extrapolation. In addition, the observed yields of the RS and WS positrons in different momentum bins are determined by fitting to $M_{\rm BC}$ distributions obtained by combining 12 hadronic ST modes together. There may be a systematic difference if instead each ST mode is fit separately and then the yields are summed. This difference is investigated by studying data collected at $\sqrt{s} = 4.682$ GeV. We compare the total ST yields with the two methods and the relative difference of 0.6% is taken as systematic uncertainty. Next, in the PID unfolding procedure, muons are treated as pions due to their similar detector responses, which may introduce a bias. To consider this systematic uncertainty, the yield of the $\Lambda_c^+ \to X\mu^+\nu_\mu$ component is estimated and the fake rates of muons to charged positrons, pions, kaons and protons are studied by using MC samples. Then we redo the analysis procedure and take the relative difference of 0.2% as the systematic uncertainty due to the treatment of muons. Summing in quadrature, we determine the total systematic uncertainty in measuring $\mathcal{B}(\Lambda_c^+ \to Xe^+\nu_e)$ to be 2.2%.

IV. SUMMARY

Based on analyzing 4.5 fb^{-1} data taken at $\sqrt{s} = 4.600$, 4.612, 4.628, 4.640, 4.661, 4.682 and 4.698 GeV with the BESIII detector at the BEPCII collider, the inclusive SL decay $\Lambda_c^+ \to Xe^+\nu_e$ was investigated. The BF of the decay is measured to be $\mathcal{B}(\Lambda_c^+ \to Xe^+\nu_e) = (4.06 \pm 0.10_{\rm stat} \pm 0.09_{\rm syst})\%$. Combining the lifetime of the Λ_c^+ baryon $\tau_{\Lambda_c^+} = (202.4 \pm 3.1) \times 10^{-15}$ s [3], we obtain the decay width $\Gamma(\Lambda_c^+ \to Xe^+\nu_e) = (2.006 \pm 0.073) \times 10^{11}\ {\rm s}^{-1}$. The charge-averaged value for D inclusive SL decay width is determined to be $\bar{\Gamma}(D \to Xe^+\nu_e) = (1.567 \pm 0.020) \times 10^{11}\ {\rm s}^{-1}$ [3]. Hence, the ratio of the inclusive SL decay width for the Λ_c^+ and D is

$$\frac{\Gamma(\Lambda_c^+ \to Xe^+\nu_e)}{\bar{\Gamma}(D \to Xe^+\nu_e)} = 1.28 \pm 0.05,$$

which is consistent but greatly improved compared with the previous published result $\Gamma(\Lambda_c^+ \to \Lambda e^+\nu_e)/\bar{\Gamma}(D \to Xe^+\nu_e) = 1.26 \pm 0.12$ [8]. At a confidence level of 95%, the determined ratio, $\Gamma(\Lambda_c^+ \to \Lambda e^+\nu_e)/\bar{\Gamma}(D \to Xe^+\nu_e) = 1.28 \pm 0.05$, is consistent with the value of 1.2 predicted from the heavy quark expansion [11] but disfavors the value of 1.67 predicted from the effective-quark method [9,10].

ACKNOWLEDGMENTS

The BESIII Collaboration thanks the staff of BEPCII and the IHEP computing center for their strong support. This work is supported in part by National Key R&D Program of China under Contracts No. 2020YFA0406400, No. 2020YFA0406300; National Natural Science Foundation of China (NSFC) under Contracts Nos. 11635010, 11735014, 11835012, 11935015, 11935016, 11935018, 11961141012, 12022510, 12025502, 12035009, 12035013, 12192260, 12192261, 12192262, 12192263, 12192264, 12192265; the Chinese Academy of Sciences (CAS) Large-Scale Scientific Facility Program; Joint Large-Scale Scientific Facility Funds of the NSFC and CAS under Contract No. U1832207; 100 Talents Program of CAS; The Institute of Nuclear and Particle Physics (INPAC) and Shanghai Key Laboratory for Particle Physics and Cosmology; ERC under Contract No. 758462; European Union's Horizon 2020 research and innovation programme under Marie Sklodowska-Curie grant agreement under Contract No. 894790; German Research Foundation DFG under Contracts No. 443159800, Collaborative Research Center CRC 1044, GRK 2149; Istituto Nazionale di Fisica Nucleare, Italy; Ministry of Development of Turkey under Contract No. DPT2006K-120470; National Science and Technology fund; National Science Research and Innovation Fund (NSRF) via the Program Management Unit for Human Resources & Institutional Development, Research and Innovation under Contract No. B16F640076; STFC (United Kingdom); Suranaree University of Technology (SUT), Thailand Science Research and Innovation (TSRI), and National Science Research and Innovation Fund (NSRF) under Contract No. 160355; The Royal Society, UK under Contracts No. DH140054, No. DH160214; The Swedish Research Council; U.S. Department of Energy under Contract No. DE-FG02-05ER41374.

TABLE IV. The PID efficiency matrix A_{PID} (in %) for $0.50 < p < 0.55$ GeV/c.

$P_{a\to b}$ (%)	$a = e$	$a = \pi$	$a = K$	$a = p$
$b = e$	95.17	0.61	0.43	0.00
$b = \pi$	6.96	93.80	0.04	0.01
$b = K$	0.78	0.07	94.42	0.01
$b = p$	0.04	0.00	0.01	97.80

APPENDIX: TABLES FOR A_{TRK} AND EFFICIENCY-CORRECTED YIELDS

Table IV shows an example of the PID efficiency matrix A_{PID} for the momentum region within $0.50 < p < 0.55$ GeV/c. Table V shows the tracking efficiency matrix A_{TRK} of positrons for each of the momentum bins. Table VI shows the efficiency-corrected positron yields in each of the momentum bins and their correlation coefficients.

TABLE V. The tracking efficiency matrix A_{TRK} for positrons. The column gives the true momentum bins j, while the row gives the reconstructed bin i.

A_{TRK} $(e\|i,j)$	1	2	3	4	5	6	7	8	9	10	11	12	13	14	15	16
1	0.7223	0.0338	0.0089	0.0058	0.0037	0.0029	0.0028	0.0024	0.0024	0.0022	0.0022	0.0022	0.0030	0.0032	0.0036	0.0009
2	0.0174	0.7359	0.0383	0.0097	0.0055	0.0041	0.0034	0.0033	0.0031	0.0027	0.0027	0.0034	0.0029	0.0034	0.0067	0.0105
3	0.0008	0.0139	0.7372	0.0389	0.0106	0.0063	0.0047	0.0041	0.0035	0.0031	0.0031	0.0032	0.0029	0.0031	0.0032	0.0017
4	0.0004	0.0008	0.0154	0.7355	0.0396	0.0106	0.0067	0.0051	0.0041	0.0036	0.0039	0.0029	0.0033	0.0038	0.0039	0.0012
5	0.0002	0.0003	0.0006	0.0148	0.7311	0.0412	0.0116	0.0070	0.0054	0.0047	0.0045	0.0035	0.0037	0.0037	0.0033	0.0014
6	0.0001	0.0003	0.0002	0.0007	0.0155	0.7248	0.0432	0.0118	0.0071	0.0056	0.0045	0.0038	0.0038	0.0050	0.0034	0.0043
7	0.0002	0.0002	0.0002	0.0003	0.0005	0.0173	0.7175	0.0455	0.0118	0.0077	0.0054	0.0049	0.0042	0.0045	0.0039	0.0028
8	0.0001	0.0001	0.0001	0.0002	0.0003	0.0008	0.0180	0.7125	0.0481	0.0120	0.0080	0.0056	0.0050	0.0044	0.0062	0.0014
9	0.0001	0.0001	0.0001	0.0002	0.0002	0.0004	0.0008	0.0196	0.7069	0.0507	0.0126	0.0084	0.0054	0.0048	0.0037	0.0018
10	0.0001	0.0001	0.0000	0.0001	0.0001	0.0002	0.0004	0.0006	0.0200	0.7043	0.0536	0.0119	0.0083	0.0047	0.0045	0.0020
11	0.0000	0.0000	0.0000	0.0001	0.0001	0.0001	0.0002	0.0003	0.0006	0.0208	0.6982	0.0580	0.0129	0.0099	0.0093	0.0047
12	0.0000	0.0000	0.0000	0.0001	0.0001	0.0001	0.0002	0.0002	0.0005	0.0004	0.0223	0.7041	0.0631	0.0117	0.0107	0.0064
13	0.0000	0.0000	0.0000	0.0000	0.0001	0.0000	0.0001	0.0001	0.0002	0.0003	0.0006	0.0213	0.6950	0.0682	0.0146	0.0046
14	0.0000	0.0000	0.0000	0.0000	0.0001	0.0000	0.0000	0.0001	0.0001	0.0002	0.0002	0.0003	0.0218	0.6997	0.0823	0.0077
15	0.0000	0.0000	0.0000	0.0000	0.0000	0.0000	0.0000	0.0000	0.0001	0.0001	0.0002	0.0003	0.0003	0.0228	0.7165	0.0712
16	0.0000	0.0000	0.0000	0.0000	0.0000	0.0000	0.0000	0.0000	0.0000	0.0001	0.0001	0.0001	0.0001	0.0005	0.0223	0.6855

TABLE VI. The efficiency-corrected positron yields $N_e^{\mathrm{prod}}(i)$ in each of the momentum bins and their correlation coefficients.

Bins	$N_e^{\mathrm{prod}}(i)$	1	2	3	4	5	6	7	8	9	10	11	12	13	14	15
1	244 ± 49															
2	308 ± 39	−0.07														
3	371 ± 40	−0.00	−0.07													
4	437 ± 38	−0.01	−0.00	−0.07												
5	524 ± 36	−0.02	−0.01	−0.00	−0.07											
6	491 ± 35	0.00	−0.02	−0.01	−0.00	−0.08										
7	513 ± 37	−0.00	0.00	−0.02	−0.01	−0.00	−0.09									
8	395 ± 32	−0.00	−0.00	0.00	−0.02	−0.01	−0.00	−0.09								
9	347 ± 28	−0.00	−0.00	−0.00	0.00	−0.02	−0.01	−0.00	−0.09							
10	305 ± 26	0.01	−0.00	−0.00	−0.00	0.00	−0.02	−0.01	−0.00	−0.10						
11	199 ± 21	−0.01	0.01	−0.00	−0.00	−0.00	0.00	−0.02	−0.01	0.00	−0.10					
12	89 ± 16	0.01	−0.01	0.01	−0.00	−0.00	−0.00	0.00	−0.02	−0.01	0.00	−0.11				
13	68 ± 12	−0.01	0.01	−0.01	0.01	−0.00	−0.00	−0.00	0.00	−0.02	−0.01	0.00	−0.11			
14	29 ± 8	0.00	−0.01	0.01	−0.01	0.01	−0.00	−0.00	−0.00	0.00	−0.01	−0.01	0.01	−0.11		
15	9 ± 5	−0.01	0.00	−0.01	0.01	−0.01	0.01	−0.00	−0.00	−0.00	0.00	−0.02	−0.01	0.01	−0.13	
16	4 ± 3	0.00	−0.01	0.00	−0.01	0.01	−0.01	0.01	0.00	−0.00	−0.00	0.00	−0.01	−0.01	0.01	−0.10

[1] B. Knapp *et al.*, Phys. Rev. Lett. **37**, 882 (1976).
[2] G. S. Abrams *et al.* (Mark II Collaboration), Phys. Rev. Lett. **44**, 10 (1980).
[3] P. A. Zyla *et al.* (Particle Data Group), Prog. Theor. Exp. Phys. **2020**, 083C01 (2020) and 2021 online update.
[4] M. Ablikim *et al.* (BESIII Collaboration), Chin. Phys. C **44**, 040001 (2020).
[5] H. B. Li and X. R. Lyu, Natl. Sci. Rev. **8**, nwab181 (2021).
[6] M. Ablikim *et al.* (BESIII Collaboration), Phys. Rev. Lett. **129**, 231803 (2022).
[7] M. Ablikim *et al.* (BESIII Collaboration), Phys. Rev. D **106**, 112010 (2022).
[8] M. Ablikim *et al.* (BESIII Collaboration), Phys. Rev. Lett. **121**, 251801 (2018).
[9] M. Gronau and J. L. Rosner, Phys. Rev. D **83**, 034025 (2011).
[10] J. L. Rosner, Phys. Rev. D **86**, 014017 (2012).
[11] A. V. Manohar and M. B. Wise, Phys. Rev. D **49**, 1310 (1994).
[12] M. Ablikim *et al.* (BESIII Collaboration), Chin. Phys. C **39**, 093001 (2015).
[13] M. Ablikim *et al.* (BESIII Collaboration), Chin. Phys. C **46**, 113003 (2022).
[14] M. Ablikim *et al.* (BESIII Collaboration), Nucl. Instrum. Methods Phys. Res., Sect. A **614**, 345 (2010).
[15] K. X. Huang *et al.*, Nucl. Sci. Tech. **33**, 142 (2022).
[16] X. Li *et al.*, Radiat. Detect. Technol. Methods **1**, 13 (2017); Y. X. Guo *et al.*, Radiat. Detect. Technol. Methods **1**, 15 (2017); P. Cao *et al.*, Nucl. Instrum. Methods Phys. Res., Sect. A **953**, 163053 (2020).
[17] S. Agostinelli *et al.* (GEANT4 Collaboration), Nucl. Instrum. Methods Phys. Res., Sect. A **506**, 250 (2003).
[18] E. A. Kurav and V. S. Fadin, Sov. J. Nucl. Phys. **41**, 466 (1985).
[19] S. Jadach, B. F. L. Ward, and Z. Was, Comput. Phys. Commun. **130**, 260 (2000); Phys. Rev. D **63**, 113009 (2001).
[20] E. Richter-Was, Phys. Lett. B **303**, 163 (1993).
[21] D. J. Lange, Nucl. Instrum. Methods Phys. Res., Sect. A **462**, 152 (2001); R. G. Ping, Chin. Phys. C **32**, 599 (2008).
[22] J. C. Chen, G. S. Huang, X. R. Qi, D. H. Zhang, and Y. S. Zhu, Phys. Rev. D **62**, 034003 (2000).
[23] R. L. Yang, R. G. Ping, and H. Chen, Chin. Phys. Lett. **31**, 061301 (2014).
[24] J. Adler *et al.* (Mark III Collaboration), Phys. Rev. Lett. **62**, 1821 (1989).
[25] H. Albrecht *et al.* (ARGUS Collaboration), Phys. Lett. B **241**, 278 (1990).
[26] M. Ablikim *et al.* (BESIII Collaboration), Phys. Rev. D **104**, 012003 (2021).
[27] M. M. Hussain and W. Roberts, Phys. Rev. D **95**, 053005 (2017); **95**, 099901 (2017).
[28] M. Pervin, W. Roberts, and S. Capstick, Phys. Rev. C **72**, 035201 (2005).
[29] T. Gutsche, M. A. Ivanov, J. G. Körner, V. E. Lyubovitskij, and P. Santorelli, Phys. Rev. D **90**, 114033 (2014); **94**, 059902(E) (2016).
[30] Stefan Meinel, Phys. Rev. D **97**, 034511 (2018).
[31] M. A. Ivanov, V. E. Lyubovitskij, J. G. Körner, and P. Kroll, Phys. Rev. D **56**, 348 (1997).
[32] C.-D. Lü, W. Wang, and F.-S. Yu, Phys. Rev. D **93**, 056008 (2016).
[33] R. N. Faustov and V. O. Galkin, Eur. Phys. J. C **76**, 628 (2016).
[34] C. F. Li, Y. L. Liu, K. Liu, C. Y. Cui, and M. Q. Huang, J. Phys. G **44**, 075006 (2017).